© 2025. Published by The Company of Biologists | Journal of Experimental Biology (2025) 228, jeb250186. doi:10.1242/jeb.250186

RESEARCH ARTICLE

Squid paralarvae turn with high agility using jets near the Reynolds number threshold for viscous domination

Ian K. Bartol[1,*], Alissa M. Ganley[1], Paul S. Krueger[2] and Joseph T. Thompson[3]

ABSTRACT

Turning is critical for survival in the ocean, as marine animals need to maneuver to capture prey, elude predators and navigate complex environments. While prior research has focused on turning performance of adult swimmers, less is known about early ontogenetic stages that locomote within lower Reynolds number (*Re*) regimes, especially young jetters. To evaluate squid paralarval turning proficiency and the role of the pulsed jet in maneuvers, recently hatched longfin inshore squid, *Doryteuthis pealeii*, swimming in a viewing chamber were studied using digital particle image velocimetry and kinematic motion analyses. Paralarvae exhibited a wide repertoire of turning behaviors, including those performed arms-first and tail-first. Paralarval turns were broader [higher mean length-specific turning radii (R/L_{mean})] and faster [higher mean angular velocity (Ω_{mean})] than those of older squids, with some turns (~8%) involving peak angular velocities (Ω_{max})>2000 deg s^{-1}. Relative to cuttlefish hatchlings, squid paralarvae exhibited lower R/L_{mean} and higher Ω_{mean} and Ω_{max}. Higher angular jet impulse produced turns of greater Ω_{mean} and total angular displacement, and R/L_{mean} and Ω_{mean} increased with higher Re_{squid}. Paralarval jets ranged from isolated vortex rings (short pulses), some of which occurred near the viscous dominated condition of Re<1, to elongated vorticity structures with and without leading edge vortex ring formation (long pulses). Despite the range of jet flows produced, strong relationships between jet length-to-diameter ratios and kinematic properties were not observed. The ability of paralarvae to produce a diversity of directed jets at low/intermediate *Re* is integral to their turning versatility and ultimately survival.

KEY WORDS: Cephalopods, Turning, Maneuverability, Velocimetry, Kinematics, Hydrodynamics

INTRODUCTION

Turning is an important component of life in the ocean, with the ability to maneuver proficiently being central to prey capture, predator avoidance, mating and courtship, and navigation through complex habitats (Domenici and Blake, 1997; Hanlon and Messenger, 2018; Howland, 1974; Weihs and Webb, 1984). Turning performance has been assessed in a wide diversity of vertebrate aquatic taxa, including fishes (Blake et al., 1995; Danos and Lauder, 2007; Fish et al., 2018; Gerstner, 1999; Parson et al., 2011; Thandiackal and Lauder, 2020; Webb, 1983; Webb and Fairchild, 2001), penguins (Harada and Tanaka, 2022; Hui, 1985), turtles (Mayerl et al., 2019; Rivera et al., 2006) and marine mammals (Fish et al., 2003; Goldbogen et al., 2013; Leahy et al., 2021; Maresh et al., 2004; Segre et al., 2019, 2022). More recently, turning performance studies have focused on marine invertebrates, such as jet-propelled gelatinous zooplankton (Dabiri et al., 2020; Gemmell et al., 2015; Sutherland et al., 2019a; Sutherland et al., 2024) and nektonic squids (Bartol et al., 2022, 2023; Ganley et al., 2023; Jastrebsky et al., 2016, 2017).

Pulsed jet propulsion is an integral locomotory mode for several distantly related marine taxa, including mollusks, urochordates and cnidarians (Gemmell et al., 2021), with modulation and control of jet flows being central to turning performance (Bartol et al., 2022, 2023; Gemmell et al., 2015). For many jetters, the generation of coherent vortex rings, either as isolated units (shorter pulses) or as the leading components of extended jets with trailing flows (longer pulses), is common during maneuvering (Bartol et al., 2022; Gemmell et al., 2015). In the colonial siphonophore *Nanomia bijuga*, multiple propulsive units (nectophores) produce coordinated, directed, high-velocity jet flows with leading ring features (e.g. fig. 3 in Sutherland et al., 2019a), with jets generated farther from the center of mass with large lever arms having the greatest influence on turning dynamics (Sutherland et al., 2019b). Jellyfish *Aurelia aurita* modulate their jet vortex rings during turns such that only a portion of the vortex ring separates from the body, altering the force balance across the animal and presumably increasing torque (Gemmell et al., 2015). Like zebrafish, *Danio rerio*, *A. aurita* begin turns with a small, rapid shift in body kinematics followed by subsequent body bending to minimize the moment of inertia (Dabiri et al., 2020).

Many cephalopods, e.g. squids, cuttlefishes, *Vampyroteuthis* and cirrate octopods, differ from other jet-propelled animals because they employ a dual-mode propulsive system, involving not only a pulsed jet but also fin motions (Anderson and Demont, 2005; Bartol et al., 2001, 2009a; Flaspohler et al., 2019; Hanlon and Messenger, 2018; Hoar et al., 1994; O'Dor, 1988). For neritic squids, such as Atlantic brief squid, *Lolliguncula brevis*, longfin inshore squid, *Doryteuthis pealeii*, and northern shortfin squid, *Illex illecebrosus*, the pulsed jet produces more angular impulse than the fins during turns (Bartol et al., 2023). While the fins and arms contribute less angular impulse, they are important for stabilization and reducing rotational resistance during turns (Bartol et al., 2022). During juvenile and adult stages, these squids also produce two jet modes while maneuvering: Jet mode I, which involves the formation of an isolated vortex ring with each jet pulse, and jet mode II, which consists of a leading-edge vortex ring structure coupled with a trailing jet with each jet pulse. The transition between these jet modes is defined by the formation number (F), which represents the physical limit of vortex ring formation (Gharib et al., 1998). In squids, F generally occurs when the jet length-to-diameter ratio based on the vorticity extent (L_ω/D_ω) is ~3 (Bartol et al., 2009a, 2022). Owing to a flexible funnel through which expelled jet flows

[1]Department of Biological Sciences, Old Dominion University, Norfolk, VA 23529, USA. [2]Department of Mechanical Engineering, University of North Texas, Denton, TX 76203, USA. [3]Department of Biology, Franklin and Marshall College, Lancaster, PA 17604, USA.

*Author for correspondence (ibartol@odu.edu)

I.K.B., 0000-0001-9006-8727; P.S.K., 0000-0001-8697-6722

Received 10 January 2025; Accepted 10 July 2025

Journal of Experimental Biology (2025) 228, jeb250186. doi:10.1242/jeb.250186

List of symbols and abbreviations

A	angular impulse
AF	arms-first swimming
COR	center of rotation
DML	dorsal mantle length
I	linear impulse
L_ω/D_ω	jet length-to-diameter ratio based on vorticity extent
R	radius of the turning path
R/*L*	length-specific turning radius
R/L_{mean}	mean length-specific turning radius
R/L_{min}	90th percentile minimum *R*/*L*
Re_{squid}	Reynolds number of the squid
Re_{jet}	Reynolds number of the jet
TF	tail-first swimming
U_{jave}	mean jet velocity
U_{jmax}	maximum jet velocity
U_{tave}	mean tangential velocity
U_{tmax}	maximum tangential velocity
θ	yaw angle
Ω	angular velocity
Ω_{max}	90th percentile maximum angular velocity
Ω_{mean}	mean angular velocity

can be vectored in any direction below the animal (Bartol et al., 2001; O'Dor, 1988), squids can turn in either an arms-first (forward) or tail-first (backward) orientation. For *L. brevis* and *I. illecebrosus*, shorter jets (jet mode I) and lower length-specific turning radii (*R*/*L*) are generally associated with arms-first turns, whereas longer and more powerful jets (jet mode II) are more common during tail-first turns (Bartol et al., 2022, 2023). Interactions between the jet, fins and highly flexible arms allow adult squids to achieve some of the lowest *R*/*L* recorded for any aquatic animal and angular velocities (Ω) that exceed 700 deg s^{-1} at their performance extremes (Jastrebsky et al., 2016, 2017).

Although the above studies have significantly advanced our understanding of turning in adult jet-propelled animals, less is known about turning at early ontogenetic stages. Early in life, jet-propelled animals produce jets at, and move within, low and intermediate Reynolds number (*Re*) regimes, where viscous forces are high or comparable to inertial effects. As *Re* decreases, viscous effects affect the flow development for starting jets, which can impact propulsive performance given the apparent role played by vortex rings (Bartol et al., 2009b; Cantwell, 1986; Herschlag and Miller, 2011; Katija et al., 2015). Indeed, there appear to be *Re* propulsion thresholds for certain jet-propelled organisms, as larval hydromedusa *Sarsia tubulosa* and paralarval longfin squid, *D. pealeii*, operate at Re_{jet} of ∼5–9 at their lowest size and activity ranges (Bartol et al., 2009b; Katija and Jiang, 2013; Katija et al., 2015). ['Paralarval' is the term used for cephalopods in the first post-embryonic phase that is planktonic and morphologically different from older conspecifics but where no metamorphosis occurs (Vidal and Shea, 2023; Young, 1988)]. Both *D. pealeii* and *S. turbulosa* exhibit similar jet wakes in early ontogeny when swimming or vertical bobbing (station holding), forming both classical and elongated vortex rings (jet mode I). At higher *Re*, greater jet velocities and later ontogenetic stages, jet mode II becomes more prominent (Bartol et al., 2008, 2009b; Katija et al., 2015). Cuttlefish *Sepia officinalis* show similar jet wake patterns, using jet mode I almost exclusively as hatchlings before transitioning to an equal mix of jet mode I and jet mode II as juveniles (Gladman and Askew, 2023).

It is unclear how the jet patterns above observed in young jetters during rectilinear swimming translate to turning, but a diversity of unsteady behaviors and maneuvers have been reported in paralarval squids. Newly hatched California market squid, *Doryteuthis opalescens* [2.5 mm dorsal mantle length (DML)], spend most of their time using a pulsed jet-and-sink motion, i.e. vertical bobbing or station holding (Vidal et al., 2018; Zeidberg and Hamner, 2002), much like *D. pealeii* paralarvae (1.8 mm DML) (Bartol et al., 2009b; Zakroff et al., 2018). In *D. opalescens* paralarvae, a key transition occurs at ∼6–7 mm DML, where paralarvae reach speeds of 562 mm s^{-1}, form schools and swim and maneuver more proficiently (Vidal et al., 2018). The development of a rocket-shaped body and larger, more powerful fins is thought to play a critical role in this life transition, as the fins are rudimentary and the mantle is more rounded in early ontogeny (Bartol et al., 2009b; von Boletzky, 1974; Shea and Vecchione, 2002; Sweeney et al., 1992; Vecchione, 1981; Vidal, 1994; Vidal et al., 2018). In addition to vertical bobbing, squid paralarvae exhibit other behaviors that involve turning, including circling, spiraling, zig-zagging and transitioning from arms-first to tail-first swimming (York and Bartol, 2016). Circling and spiraling behaviors resemble spinning and corkscrewing motions of ocean macroplankton, such as the salp *Iasis cylindrica* (Sutherland et al., 2024).

Although no prior studies focusing on turning dynamics of squid paralarvae have been performed, cuttlefish hatchlings have been examined. Using body motion tracking and digital particle image velocimetry (DPIV), Ganley et al. (2024) found that common cuttlefish, *S. officinalis*, hatchlings turn with greater Ω than dwarf cuttlefish, *Sepia bandensis*, hatchlings using high velocity/impulse jets, but that both species complete maneuvers with similar *R*/*L*. In contrast to adult squids, no differences were found in turn dynamics according to orientation, i.e. arms-first versus tail-first. Although both species use jet modes I and II, jet mode I is the preferred jet pattern for maneuvers, which presumably allows for greater control throughout the turning path (Ganley et al., 2024).

At eclosion, squid paralarvae must swim and turn effectively to find and capture food, avoid predation and undergo vertical migrations (Robin et al., 2014; Vidal and Shea, 2023; Vidal et al., 2018; Zeidberg and Hamner, 2002). They must accomplish these locomotive tasks quickly given rapidly depleting yolk reserves (Vidal et al., 2018) while contending with the physical constraints associated with low/intermediate *Re* regimes (Vogel, 2013). The present study focuses on quantifying how effective squid are at turning during the early, critical, paralarvae stage and how young squid achieve turns using their pulsed jet in low and intermediate *Re* environments. Specifically, we examined three hypotheses in longfin squid, *D. pealeii*, paralarvae. (1) Squid paralarvae will turn faster (greater Ω) but more broadly (greater *R*/*L*) than cuttlefish hatchlings and older ontogenetic stages. Given *D. pealeii* paralarval size (<2 mm DML) and high dependence on the pulsed jet (fins are rudimentary at early life stages), we expected paralarvae to reach higher Ω than their adult counterparts (>160 mm DML) and cuttlefish hatchlings (>9 mm DML), both of which should have higher moments of inertia because of their larger size. However, based on their less developed control surfaces (e.g. fins and arms), we expected squid paralarvae would turn more broadly. (2) Higher jet angular impulse (**A**) will contribute to greater Ω and total angular displacement, and higher *Re* will contribute to higher *R*/*L* and Ω. To generate fast and significant turns, higher **A** was expected. We also predicted that viscosity would aid squid paralarvae in completing tight turns, as greater viscosity should limit drift/coasting, while increases in relative inertial effects at higher *Re* should benefit paralarvae when making fast turns, as limited viscous effects promote faster swimming. (3) Both jet mode I and jet mode II will be used for paralarvae turns, and turning kinematics will correlate

with jet wake topology, with shorter jets (L_ω/D_ω<3) being associated with tight, controlled turns and longer jets (L_ω/D_ω>3) occurring more frequently with broad, fast turns. Although jet mode I is the predominant mode for squid paralarvae during station holding and cuttlefish hatchlings while swimming, we expected higher reliance on both jet modes to achieve the expected broad range of turning behaviors (e.g. tight to broad, slow to fast). Additionally, we expected shorter jets would be most advantageous for sharp turns, as they could be more precisely directed along the turning path, whereas longer, powerful jets would be beneficial for fast but broad turns where less control is required.

MATERIALS AND METHODS

Animals

Longfin inshore squid, *Doryteuthis pealeii* (Lesueur 1821), eggs were purchased from the Marine Biological Laboratory (Woods Hole, MA, USA). The eggs were maintained in free-floating 19 l buckets suspended with polyethylene foam wrapped around the upper rim within a 1700 l recirculating seawater system at 30 ppt and 22–24°C. To facilitate flow circulation, 5 cm diameter holes were drilled in the buckets and covered with 0.5 mm mesh. Upon hatching, which occurred at night, paralarvae ascended to the water surface and were transferred to experimental chambers (see below) using a pipette. Only paralarvae <24 h old post-hatching [1.8 mm DML, ∼3.5 mm total length (L)] were used in experiments. Any paralarvae remaining in the free-floating buckets after 24 h were transferred to another floating enclosure to ensure only recently hatched animals were considered for the experiment. All research protocols were approved under Old Dominion University's IACUC #21-002.

Experiments

Squid paralarvae were placed in a Plexiglas viewing chamber (10.0×6.0×2.5 cm) in groups of 5–20 individuals and allowed to acclimate for 5 min. Following acclimation, several 20 s long recording sessions were performed for each grouping of individuals, with 61 total sets of animals considered. Multiple individuals were added to the holding chamber to increase the probability of imaging turning squid within a limited field of view. Seawater in the viewing chamber was maintained at 30 ppt and 22–24°C and seeded with neutrally buoyant light reflective particles (silver-coated, hollow glass spheres, diameter 14 µm; Potters Industries, Valley Forge, PA, USA). The particles were illuminated in a 1.0–1.5 mm parasagittal plane using a dual-pulsed Evergreen HP 340 mJ pulse^{-1} PIV laser (532 nm wavelength, 15 Hz dual frequency, Quantel Laser, Bozeman, MT, USA) and laser plane optics (Beamtech, Beijing, China).

A PowerView 4MP-HS camera (2048×2048 pixels, 30 frames s^{-1}; TSI, Inc., Shoreview, MN, USA) outfitted with a Navitar 6000 series zoom lens with fine focus (Navitar, Inc., Rochester, NY, USA) was used to record illuminated particles in a 3.0×3.0 cm field of view (FOV) for DPIV applications. To record paralarvae kinematics, three Falcon cameras (Teledyne Dalsa, Inc., Waterloo, ON, Canada; 1400×1200 pixels, 100 frames s^{-1}) were positioned around the viewing chamber, two laterally and one from above. One lateral camera was outfitted with a zoom lens (VZM 450i zoom lens, Edmund Optics, Barrington, NJ, USA) for close-up views (FOV: 2.2×3.0 cm) of the paralarvae and the other lateral camera was configured with a 25 mm lens (Fujinon, Inc., Wayne, NJ, USA) for a broader FOV (6.0×8.1 cm). A 35 mm lens (Fujinon, Inc.) was used with the camera positioned above the chamber, which was important for determining paralarvae position relative to the laser sheet and to assess laser thickness. Separate lighting sources and filters were used with the DPIV and kinematic cameras. For the DPIV camera, which was illuminated using the laser described above, an optical filter allowing only laser light illumination at 532±5 nm to reach the CCD sensor was used. Halogen lights with filters to transmit red wavelengths (>600 nm) were used to illuminate the kinematic cameras. All DPIV data acquisition, camera timing and laser timing were achieved using INSIGHT 4G software and synchronizer hardware (TSI, Inc.). Paired images were collected at 15 Hz, with a time separation between paired images (Δt) of 1.0–2.0 ms. Video acquisition and recording from the Falcon cameras were achieved using a DVR Express Core2 system and CoreView software (IO Industries, London, ON, Canada).

Kinematic processing

One representative sequence from each squid (n=79) was selected for kinematic processing. The sequences chosen represented a suite of different turning behaviors, and four criteria were used in the sequence selection process: (1) the paralarvae were at least 1 cm from side walls and 3 cm above the chamber floor, (2) the paralarvae performed turns within the laser plane, (3) the total angular displacement of the turn was >7 deg, and (4) high-quality DPIV data of jet flow were present (e.g. clear jet velocity vector fields, well-developed vortical flow features). For each of the selected turning sequences, position tracking of squid body landmarks was performed using image tracking software (Hedrick, 2008). The tracking protocols were similar to those described in Jastrebsky et al. (2016), although a smaller subset of body landmarks was considered. These landmarks included: (1) the posterior end of the mantle (tail), (2) the point equidistant between the eyes, (3) the distal tip of the longest arm, (4) the widest point of the left side of the mantle and (5) the widest point of the right side of the mantle (Fig. 1A). Digitized points in the video footage were used to determine the center of rotation (COR), angular velocity (Ω) and radius of curvature of the center of rotation (R) using in-house MATLAB (MathWorks, Inc., Natick, MA, USA) routines (Fig. 1B). Data used to calculate COR and Ω were smoothed using either the mean squared error algorithm or cross-validation criterion (Walker, 1998). COR is the point in the domain of the paralarval body that moved the least during the turn. It was calculated using the approach described in Bartol et al. (2023) where COR falls on a line that is at a fixed angle (α) from the line connecting the tail tip and arm tip and that has the same length as the distance between these points (Fig. 1B). The radius of curvature of the COR trajectory (R) was determined using:

$$\frac{1}{R} = \frac{y''}{(1 + (y')^2)^{3/2}}, \quad (1)$$

where $y' = \mathrm{d}y/\mathrm{d}x = \dot{y}/\dot{x}$, $y'' = \mathrm{d}^2y/\mathrm{d}x^2 = (\dot{x}\ddot{y} - \dot{y}\ddot{x})/\dot{x}^3$, x and y are the coordinates of the COR, t is time, the over dot represents time differentiation, and the derivatives were evaluated using fourth-order accurate finite difference equations. To compare our data with those of previous studies, the radius of the turning path (R) was divided by the total length (L) of the animal to determine the length-specific turning radius (R/L). R/L_{mean} is the average of all COR radii for a given turn, divided by L, whereas Ω_{mean} is the mean angular velocity throughout the turn. To account for frame digitization error, turning radii and angular velocities for each sequence were ranked and the 90th percentile minimum R/L (R/L_{min}) and the 90th percentile maximum Ω (Ω_{max}) were determined.

Journal of Experimental Biology (2025) 228, jeb250186. doi:10.1242/jeb.250186

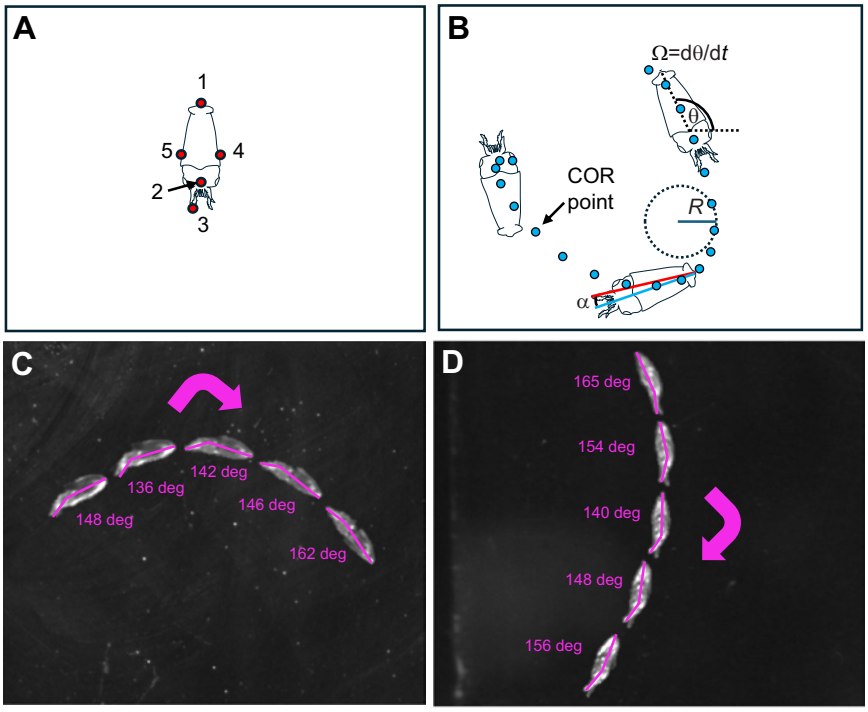

Fig. 1. Kinematic parameters, behaviors and turning paths for longfin squid, *Doryteuthis pealeii*, paralarvae. Tracking points (1, posterior end of mantle; 2, point equidistant between the eyes; 3, distal tip of longest arm; 4, widest point of left side of mantle; and 5, widest point of right side of mantle; A) and center of rotation (COR) points (B). The COR is located on a line (blue) that is at a fixed angle (α) from the line connecting the tail tip and arm tip (red) and that has the same length as the distance between these points. The distance of the COR from the tail tip and α are selected so that the COR moves the least amount during the turn. The radius (R) of the COR path was measured throughout the turn, and the numerical derivative of the animal yaw angle (θ) versus time was determined using a fourth-order finite difference formula to compute angular velocity (Ω). A tail-first (C) and arms-first (D) turning sequence, depicting body curvature with the interior angle between mantle and arms shown.

DPIV processing

Within a turning sequence, the DPIV frame where propulsive flow vorticity had completely shed from the body and where impulse was maximal was processed. This approach is appropriate because the selected image contains the cumulative history of the flow generation, and calculation of impulse (**I**) and of angular impulse (**A**) are integral methods. Although jet vortex circulation for squid paralarvae may decrease by as much as 12% between DPIV frames collected at 15 Hz (Bartol et al., 2009b), **I** and **A** are conserved following completion of the jet pulse (Saffman, 1993), and thus the time delay between DPIV measurements does not impact the assessment of these quantities. Given that illuminated regions of the squid body can lead to erroneous velocity vectors, the brightly lit squid body was removed from the flow field using the polygon masking feature in INSIGHT 4G. Velocity and vorticity fields were calculated using INSIGHT 4G software, and all data plots were generated using Tecplot 360 (Tecplot, Bellevue, WA, USA). A recursive Nyquist grid engine and Fast Fourier Transform (FFT) correlator were used to determine particle displacement, with a first pass interrogation window size of 64×64 pixels and a second pass interrogation window size of 32×32 pixels. Vector local validation was performed using the median test with a neighborhood of 5×5; vector field conditioning and smoothing were completed with recursive local mean filling and low pass filtering with sigma=0.8. Because it was not possible to reliably resolve flows around the small fins while also imaging the much larger, higher magnitude jet flow, fin flows were not considered for this study. Velocity vector fields were imported into in-house MATLAB routines to determine bulk wake properties that included average and peak jet velocity (U_{jave}, U_{jmax}), jet length (L_ω), jet diameter (D_ω), impulse (**I**) and angular impulse (**A**). Vorticity-based jet length (L_ω) was the extent over which the jet vorticity field was above a specified threshold (20% of maximum vorticity). Jet diameter (D_ω) was the distance between vorticity cores (regions where vorticity was >90% of peak jet vorticity) perpendicular to the jet centerline. Equations used to calculate **I** and **A** were identical to those used in Ganley et al. (2024). Impulse was calculated using the following equation:

$$\frac{\mathbf{I}}{\rho} = \pi\hat{\mathbf{z}}\int_{\text{jet}} \omega_\theta r^2 \mathrm{d}r\mathrm{d}z, \tag{2}$$

where ω_θ is the azimuthal component of vorticity, r is the radial coordinate relative to the jet centerline, z is the longitudinal coordinate along the jet axis, ρ is fluid density and $\hat{\mathbf{z}}$ is a unit vector aligned with the jet centerline and oriented in the direction of the jet flow. By Newton's third law, the impulse applied to the squid is in the $-\hat{\mathbf{z}}$ direction. Angular impulse was computed from:

$$\frac{\mathbf{A}_0}{\rho} = \frac{1}{3}\int \mathbf{x}\times\mathbf{x}\times\boldsymbol{\omega}\mathrm{d}V, \tag{3}$$

where ρ is fluid density, $\mathbf{x}$ is the position vector relative to an arbitrary origin, $\boldsymbol{\omega} = \nabla\times\mathbf{u}$ is the vorticity vector, $\mathbf{u}$ is the fluid velocity vector, '×' is the vector cross-product, and the integral is taken over the volume of the jet vorticity. For an axisymmetric jet with the jet centerline in the same plane as the squid paralarva centroid, the angular impulse computed relative to the centroid of the squid (**A**) reduces to:

$$\frac{\mathbf{A}}{\rho} = \frac{r_0 I}{\rho}\hat{\mathbf{z}}\times\hat{\mathbf{r}}, \tag{4}$$

where $\hat{\mathbf{r}}$ is the unit vector orthogonal to the jet centerline pointing in the direction of the squid, r_0 is the distance between the jet centerline and the squid centroid measured perpendicular to the jet centerline, and $I=|\mathbf{I}|$ is the magnitude of the impulse vector. By Newton's third law, the angular impulse applied to the squid is opposite to **A**.

The laser sheet thickness exceeded the funnel diameter. Thus, to address underestimates of jet velocity and peak vorticity resulting from depth averaging across the laser sheet, a deconvolution routine was employed. A general description of the process is included below with further information provided in Bartol et al. (2009b).

The depth averaging effect was expressed as a convolution operation:

$$\langle f \rangle = \int_0^\infty k(r) f\,(z,r)\mathrm{d}r, \tag{5}$$

where f is the data field being convolved (averaged) and k is the convolution kernel. For axial velocity, we set f=u_z and k=1 within the laser sheet and k=0 elsewhere, giving:

$$\langle u_z \rangle(z,r) = \int_r^{\sqrt{r^2+(T/2)^2}} u_z\,(z,r')\mathrm{d}r', \tag{6}$$

where $\langle u_z \rangle$ is the convolved (measured) axial velocity, u_z is the actual axial jet velocity and T is the thickness of the laser sheet. For the radial velocity (u_r), we set k=cos[$\theta_r(\tau)$] within the laser sheet and k=0 elsewhere. $\theta_r(\tau)$ is the angle between the 3D radial direction relative to the jet axis and the vertical plane of the center of the laser sheet at location τ within the laser sheet. Using this convolution kernel, the convolution operation for the radial velocity becomes:

$$\langle u_r \rangle(z,r) = \int_r^{\sqrt{r^2+(T/2)^2}} \cos[\theta_r(r')]\; u_r\,(z,r')\mathrm{d}r'. \tag{7}$$

To remove convolution reductions in velocity data and impulse values due to averaging over the laser sheet thickness T, the data were deconvolved using an iterative algorithm that reproduced the actual velocity components u_z and u_r to within 1% of peak jet velocity. Deconvolution of all velocity fields was used to obtain more accurate values of U_{jave}, U_{jmax}, **I** and **A**.

Reynolds number

Reynolds numbers (Re) were calculated using two definitions:

$$Re_{squid} = \frac{U_{tmax} L}{\nu}, \tag{8}$$

$$Re_{jet} = \frac{U_{jmax} D}{\nu}, \tag{9}$$

where Re_{squid} is the animal-based Reynolds number, Re_{jet} is the jet-based Reynolds number, U_{tmax} is the maximum tangential velocity achieved through the turning sequence, U_{jmax} is the maximum jet velocity used through the turning sequence, L is the total length of the animal, D is diameter of the squid funnel when fully expanded and ν is kinematic viscosity of the fluid.

RESULTS

Behavior

Turning sequences of 79 paralarval *D. pealeii* were considered (n=79). A wide diversity of turns was captured. Most of the turns were performed tail-first (TF, 95%) as opposed to arms-first (AF, 5%). Although spiraling turns involving multi-plane rotation were observed, they were excluded from analysis because flow features could not be captured with the planar DPIV approach. The rudimentary fins were often active during turns, but their movements had, in most cases, limited effect on the maneuvering behavior relative to the more powerful jet. In contrast, the arms, which are more muscular than the fins, frequently served as a posterior (TF) or anterior (AF) rudder/steering mechanism to aid the turn (e.g. Fig. 1C,D). In some sequences, active sweeps of the arms occurred that together with the rotating body induced water movement (see below). For many sequences, the mantle, head and arms formed an arc aligned with the turn trajectory (Fig. 1C,D).

Kinematics

All values that follow are reported as means±1 s.e.m. Mean total angular displacement of turns was 61.53±4.44 deg, with a range of angular displacement from 7.14 to 205.19 deg. Paralarvae were capable of rapid turns; mean angular velocity (Ω_{mean}) was 473.69±29.17 deg s^{-1} (range: 84.05 to 1482.02 deg s^{-1}) and mean peak angular velocity (Ω_{max}) was 1060.44±124.06 deg s^{-1} (range: 222.94 deg s^{-1} to 7657.50 deg s^{-1}). Approximately 8% of recorded turns involved Ω_{max}>2000 deg s^{-1}. Length-specific turning radii were modest, with mean R/L_{mean}=0.43±0.06 (range: 0.03 to 2.84) and mean R/L_{min}=0.022±0.0036 (range: 0.00039 to 0.19). No clear relationship between Ω_{mean} and R/L_{mean} was detected (Fig. 2A). However, a significant linear regression between Ω_{mean} and total angular displacement was present (Fig. 2B). Mean tangential velocity (U_{tave}) and maximum tangential velocity (U_{tmax}) during turning sequences were 15.6±1.6 mm s^{-1} (range 2.1 to 80.4 mm s^{-1}) and 37.5±3.8 mm s^{-1} (range 3.7 to 193.1 mm s^{-1}), respectively.

Flow dynamics

During turning sequences, jet flow ranged from isolated vortex rings (jet mode I) to elongated vorticity structures with and without evidence of leading-edge vortex ring formation (jet mode II) (Fig. 3). Mean L_ω/D_ω was 3.23±0.14, ranging from 1.79 to 8.30. For many jet sequences, animal rotation induced water motion, resulting in a significant drag signature that sometimes interacted with jet flows (Fig. 4). As mentioned above, arm bending was sometimes used to help steer the turn, which, together with the body, produced prominent flow profiles (e.g. Fig. 4A/E,B/F,C/G). Mean jet velocity (U_{jave}) was 22.26±1.28 mm s^{-1} (range: 5.97 to 71.60 mm s^{-1}), whereas mean maximum jet velocity (U_{jmax}) was 38.41±2.16 mm s^{-1} (range: 12.86 to 128.89 mm s^{-1}). The deconvolution correction increased velocities significantly, with non-corrected U_{jave}=8.78±0.29 mm s^{-1} and maximum U_{jmax}=15.05±0.48 mm s^{-1}. The mean of the absolute value of angular impulse ($|\mathbf{A}|_{ave}$) for turning sequences was 2.28×10^{-10}±4.09×10^{-11} kg m^2 s^{-1} (range: 7.98×10^{-12} to 2.01×10^{-9} kg m^2 s^{-1}). During turns, paralarvae operated at Re_{squid}=14–712 and Re_{jet}=3–31 (Fig. 5A,B). Approximately 8% of the turning sequences involved isolated vortex rings (L_ω/D_ω<4) at Re_{jet}<5, with 24% of jets falling below a Re_{jet} of 6 (Fig. 5B), which is near or below the lower range of Re_{jet} reported for other jet-propelled animals.

Relationships between kinematics and jet properties

Mean angular velocity (Ω_{mean}) and total angular displacement were dependent on angular impulse ($|\mathbf{A}|$) (Fig. 6A,B). Expected patterns between kinematic properties and jet features were observed in many sequences, such as shorter jets (low L_ω/D_ω) contributing to tight turns (low R/L_{mean}) (Fig. 7A) and longer jets (high L_ω/D_ω) contributing to fast turns (high Ω_{mean}) (Fig. 7D). However, other sequences did not follow predictions, with some sequences involving low L_ω/D_ω and high Ω_{mean} (Fig. 7B) and high L_ω/D_ω and low R/L_{mean} (Fig. 7E). Similarly, many sequences involved high $|\mathbf{A}|$ and high Ω_{mean} (Fig. 7C) or low $|\mathbf{A}|$ and low R/L_{mean} (Fig. 7F) as predicted, but other sequences diverged from our hypothesized trends, with high $|\mathbf{A}|$ sometimes contributing to low R/L_{mean} (Fig. 7G). Because of this variability in turning behaviors, significant relationships between Ω and L_ω/D_ω (Fig. 6D) or R/L and $|\mathbf{A}|$ were not detected. However, R/L_{mean} and Ω_{mean} did increase

Journal of Experimental Biology (2025) 228, jeb250186. doi:10.1242/jeb.250186

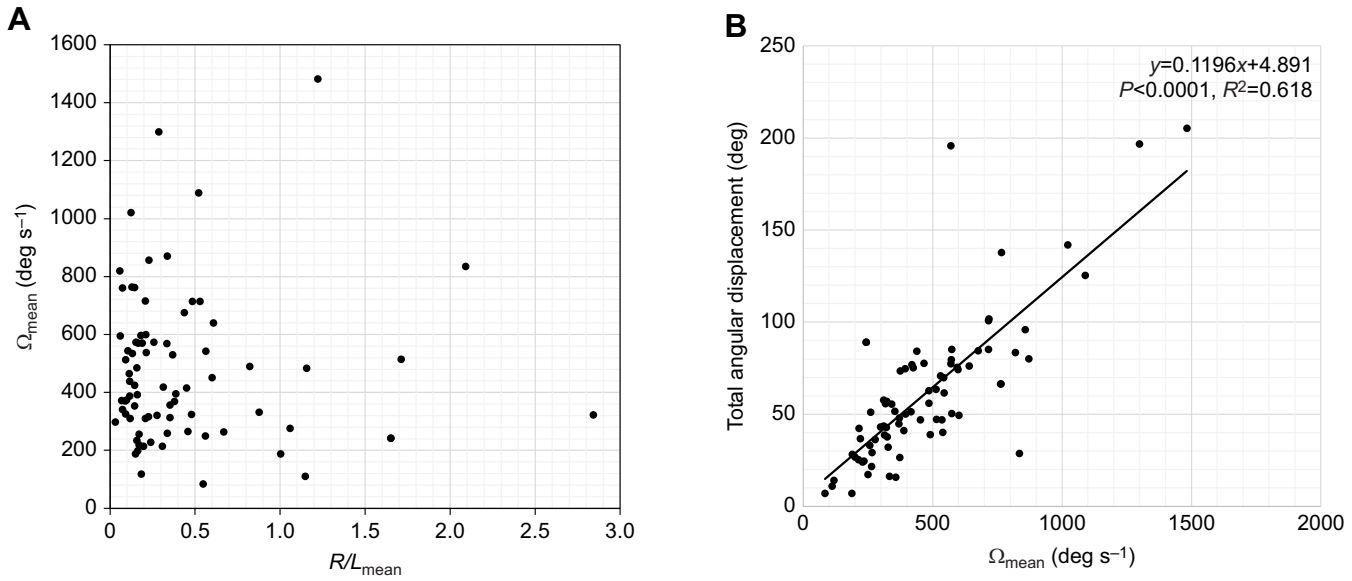

Fig. 2. Turning kinematics in paralarval *D. pealeii*. (A) Mean angular velocity (Ω_{mean}) versus mean length-specific turning radius (R/L_{mean}). (B) Total angular displacement versus Ω_{mean}.

significantly with higher Re_{squid} (Fig. 5C,D), and a significant but weak (low R^2) linear relationship between R/L_{mean} and L_ω/D_ω was present (Fig. 6C).

DISCUSSION

This study is the first to examine the turning performance of paralarval squid, which swim and produce jet flows in a low/intermediate *Re* realm (Re_{jet}=3–31, Re_{squid}=14–712). The results indicate that paralarval *D. pealeii* can turn at high angular velocity (Ω) and moderate turning radii (R/L) using their vectored, pulsed jet. Approximately 8% of turns involved Ω_{max}>2000 deg s^{-1}, with one paralarva reaching the fastest Ω reported for any aquatic animal (>7600 deg s^{-1}), outperforming even fast-turning fishes, such as wrasse, surgeonfish, damselfish and butterflyfish (Gerstner, 1999). Higher jet angular impulse (**A**) led to greater Ω and angular displacement, and Re_{squid} influenced R/L and Ω. Both jet modes I and II were observed during turns, with some vortex ring-based jets occurring near and below the *Re* threshold of ∼5–9 reported previously in theoretical and experimental studies of other jet-propelled animals (Herschlag and Miller, 2011; Katija and Jiang, 2013; Katija et al., 2015). Unexpectedly, L_ω/D_ω was not a good predictor of R/L or Ω.

Turning performance

Relative to cuttlefish hatchlings, squid paralarvae are more proficient overall at turning. Using similar techniques and measurements to those described in the present study, Ganley et al. (2024) reported R/L_{mean}=0.64–0.67 and R/L_{min}=0.024 for

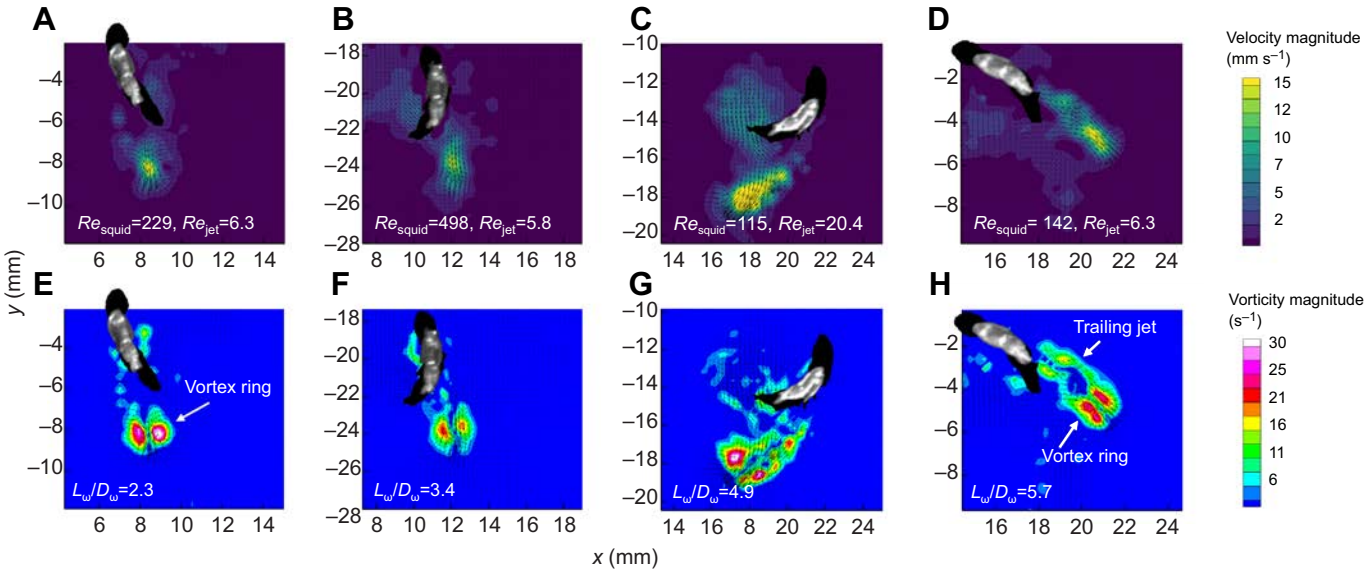

Fig. 3. Jet flow during turning sequences in paralarval *D. pealeii*. (A–D) Velocity magnitude and (E–H) corresponding vorticity magnitude for turns (before deconvolution). Jet length-to-diameter ratio based on the vorticity extent (L_ω/D_ω) is included in each vorticity plot, with increasing L_ω/D_ω shown from left to right. Position of the squid in the frame is depicted, along with silhouettes of the squid location 0.05 s before and after the frame to demonstrate turning direction. Re_{squid}, animal-based Reynolds number; Re_{jet}, jet-based Reynolds number.

Journal of Experimental Biology (2025) 228, jeb250186. doi:10.1242/jeb.250186

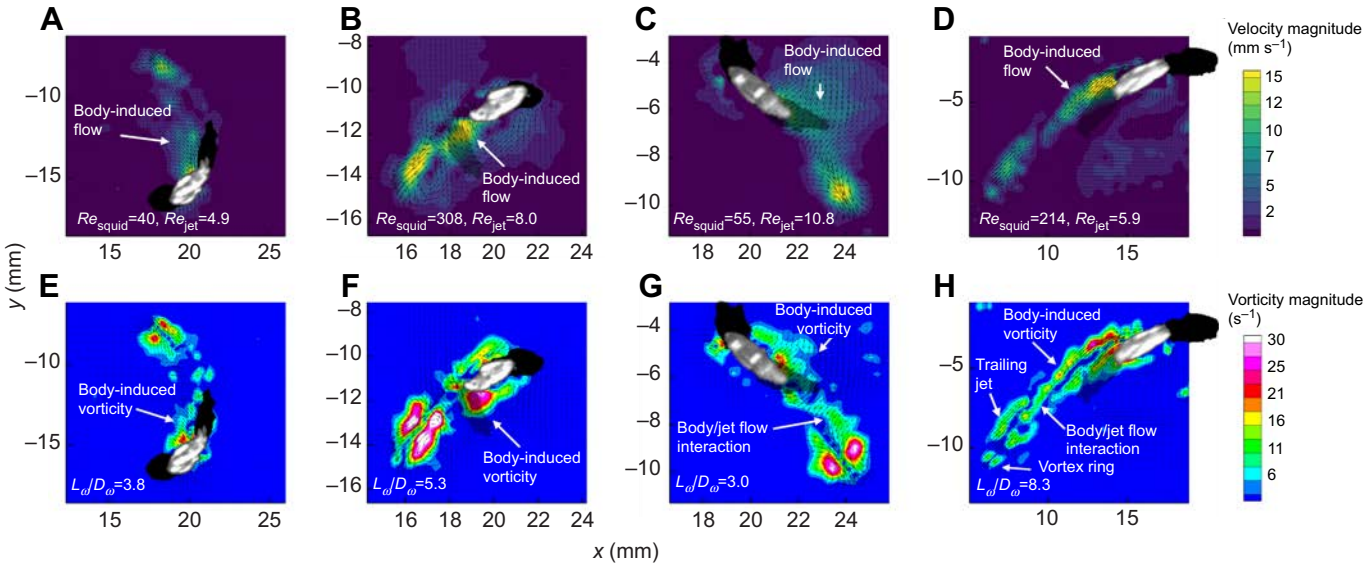

Fig. 4. Interaction of body rotation and jet flow during jet sequences in paralarval *D. pealeii*. (A–D) Velocity magnitude and (E–H) corresponding vorticity magnitude for turns (before deconvolution). Body-induced flow/vorticity are highlighted. Position of the squid in the frame is depicted, along with silhouettes of the squid location 0.05 s before and after the frame to demonstrate turning direction. Re_{squid}, animal-based Reynolds number; Re_{jet}, jet-based Reynolds number; L_ω/D_ω, jet length-to-diameter ratio based on the vorticity extent.

dwarf cuttlefish, *S. bandensis*, and common cuttlefish, *S. officinalis*. Squid paralarvae in this study trended toward lower R/L_{mean} (0.43) and R/L_{min} (0.022) (Fig. 8C,D). Given cuttlefish hatchlings are neutrally buoyant (aids station holding), have larger fins (more control surfaces for position adjustments) and presumably are more advanced developmentally than planktonic paralarvae (Hanlon and Messenger, 2018; Vidal and Shea, 2023), it is surprising that squid paralarvae exhibited tighter routine turns than young cuttlefish. Significant behavioral and cognitive plasticity/development occur as cuttlefish transition from the first to the second month of life (Dickel et al., 1998, 2001, 2013; Hanlon and Messenger, 2018; O'Brien et al., 2017). Thus, although cuttlefish may be more advanced than paralarvae in many areas, such as vision and camouflage, neuromuscular control for turning may take longer,

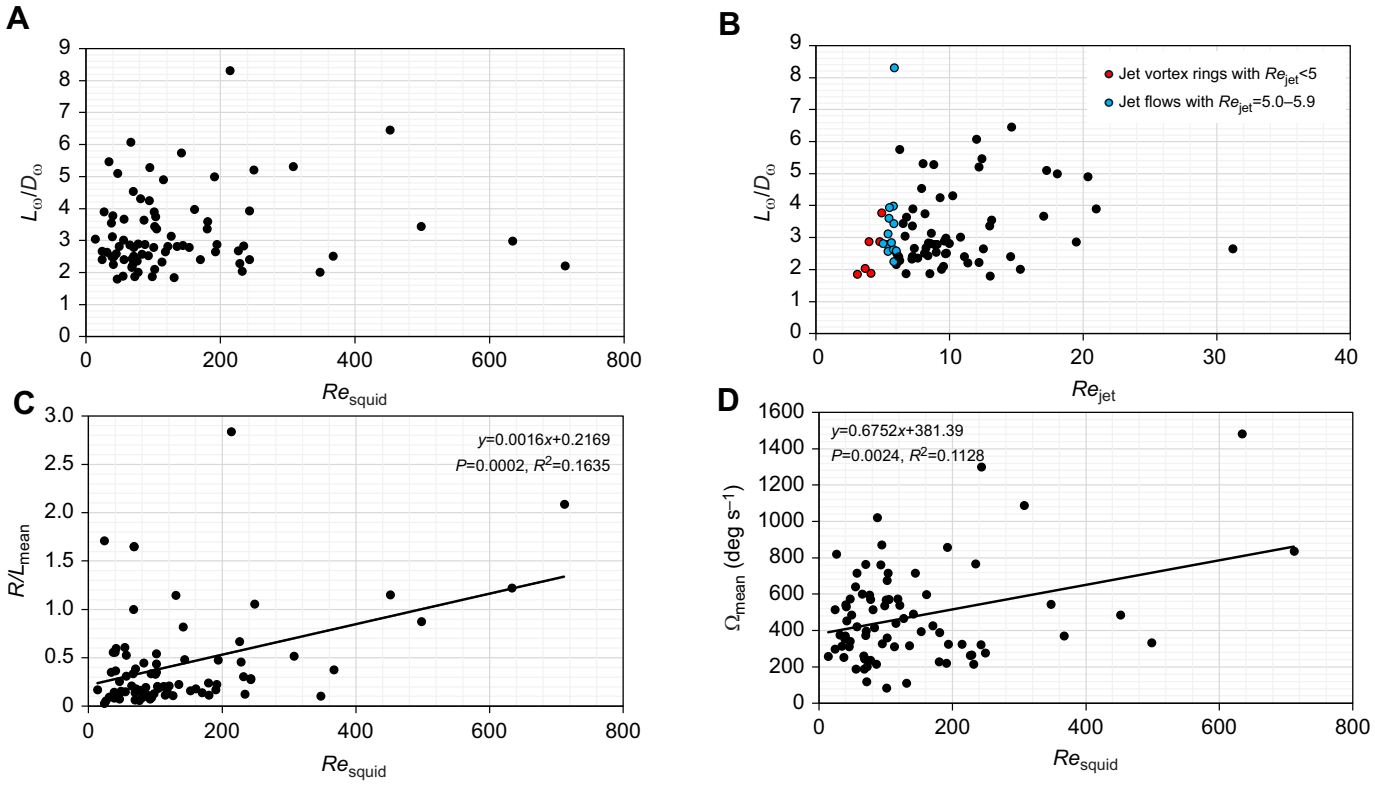

Fig. 5. Reynolds number (*Re*) versus jet properties and kinematic variables for paralarval *D. pealeii* turns. Jet length-to-diameter ratios based on the vorticity extent (L_ω/D_ω) versus Re_{squid} (A) and Re_{jet} (B). Mean length-specific turning radius (R/L_{mean}; C) and mean angular velocity (Ω_{mean}; D) versus Re_{squid}.

Journal of Experimental Biology (2025) 228, jeb250186. doi:10.1242/jeb.250186

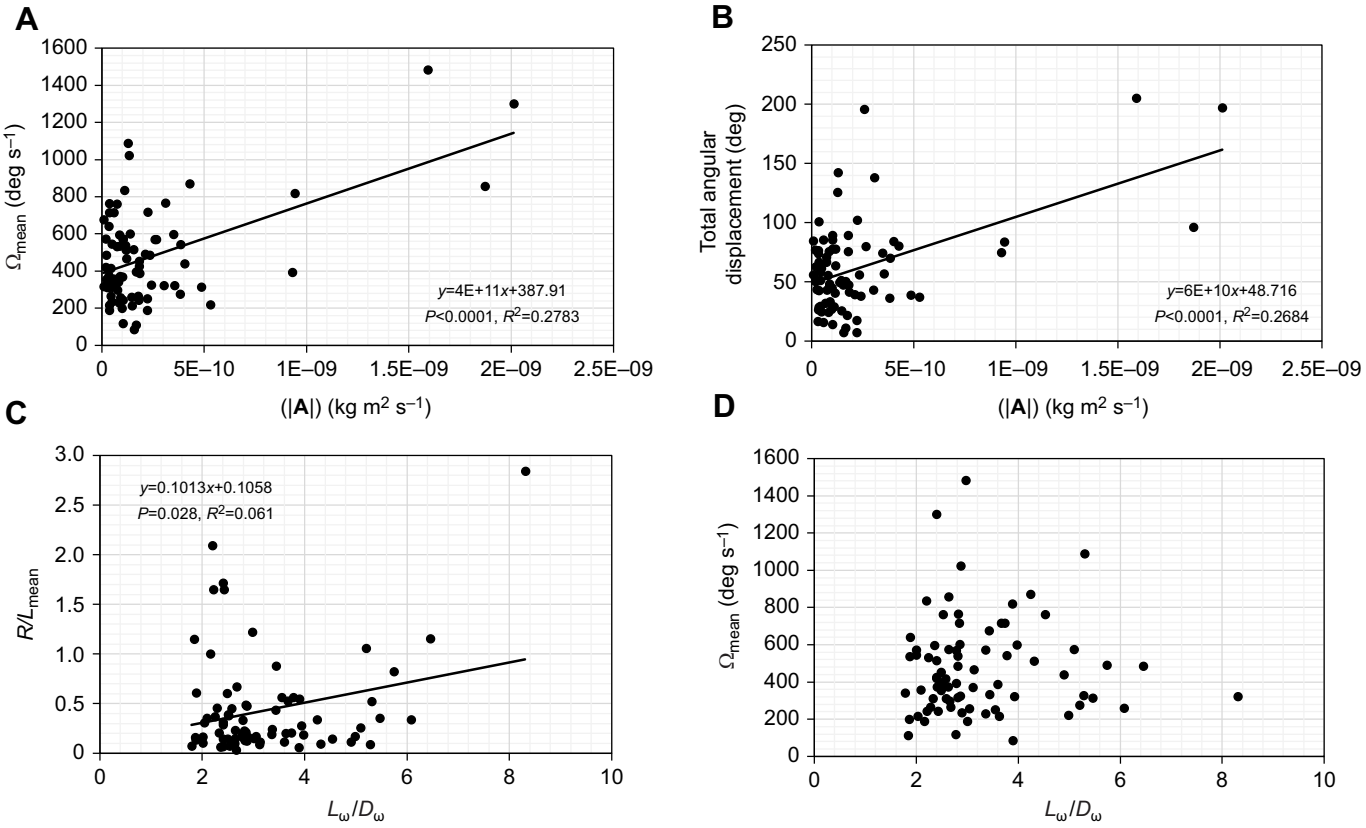

Fig. 6. Relationships between jet properties and kinematic variables for paralarval *D. pealeii*. Mean angular velocity (Ω_{mean}; A) and total angular displacement (B) versus the absolute value of angular impulse (|**A**|). Mean length-specific turning radius (R/L_{mean}; C) and mean angular velocity (Ω_{mean}; D) versus jet length-to-diameter ratio based on the vorticity extent (L_ω/D_ω).

with significant development potentially occurring in the second month of life. Interestingly, cuttlefish hatchlings can turn as tightly as squid paralarvae at their performance extremes (R/L_{min} are similar between the two groups) (Fig. 8D). Therefore, the differences in R/L_{mean} may simply reflect a preference toward broader routine turns, as frequent tight turns may be less necessary

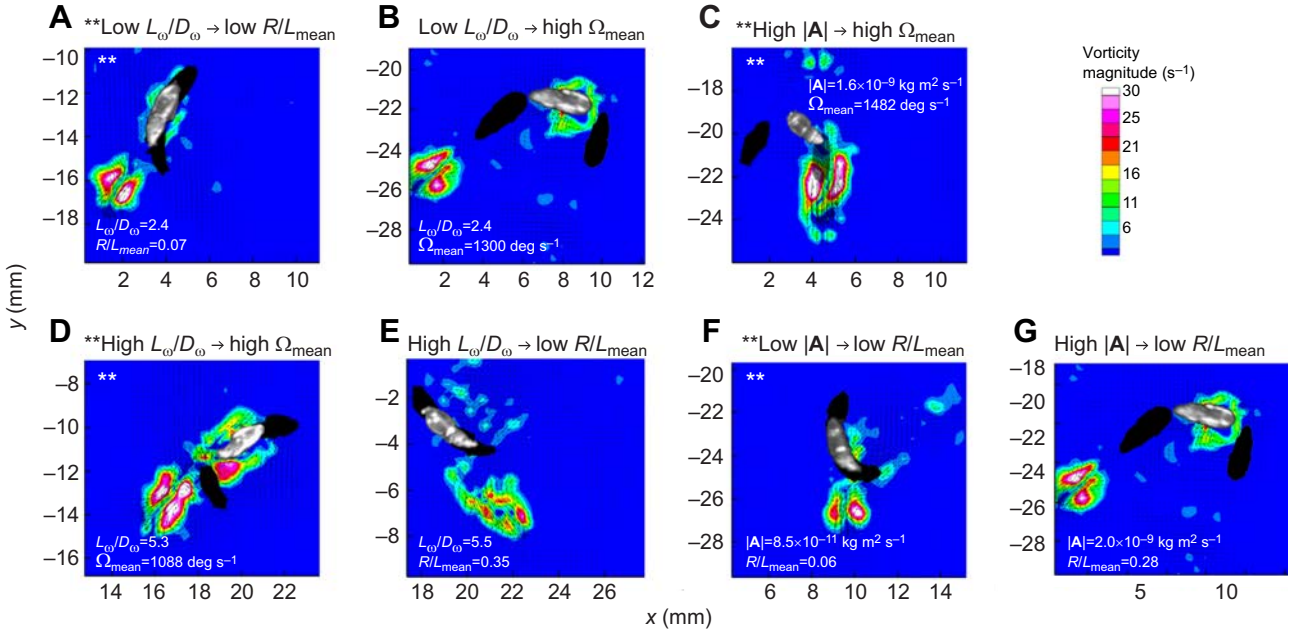

Fig. 7. Vorticity magnitude for paralarval *D. pealeii* turns (before deconvolution). Panels with asterisks (A,C,D,F) depict expected patterns, whereas those without (B,E,G) represent unexpected patterns. Position of the squid in the frame is shown, along with silhouettes of the squid location 0.05 s before and after the frame to demonstrate turning direction. L_ω/D_ω, jet length-to-diameter ratio based on the vorticity extent; R/L_{mean}, mean length-specific turning radius; Ω_{mean}, mean angular velocity; |**A**|, absolute value of angular impulse.

Journal of Experimental Biology (2025) 228, jeb250186. doi:10.1242/jeb.250186

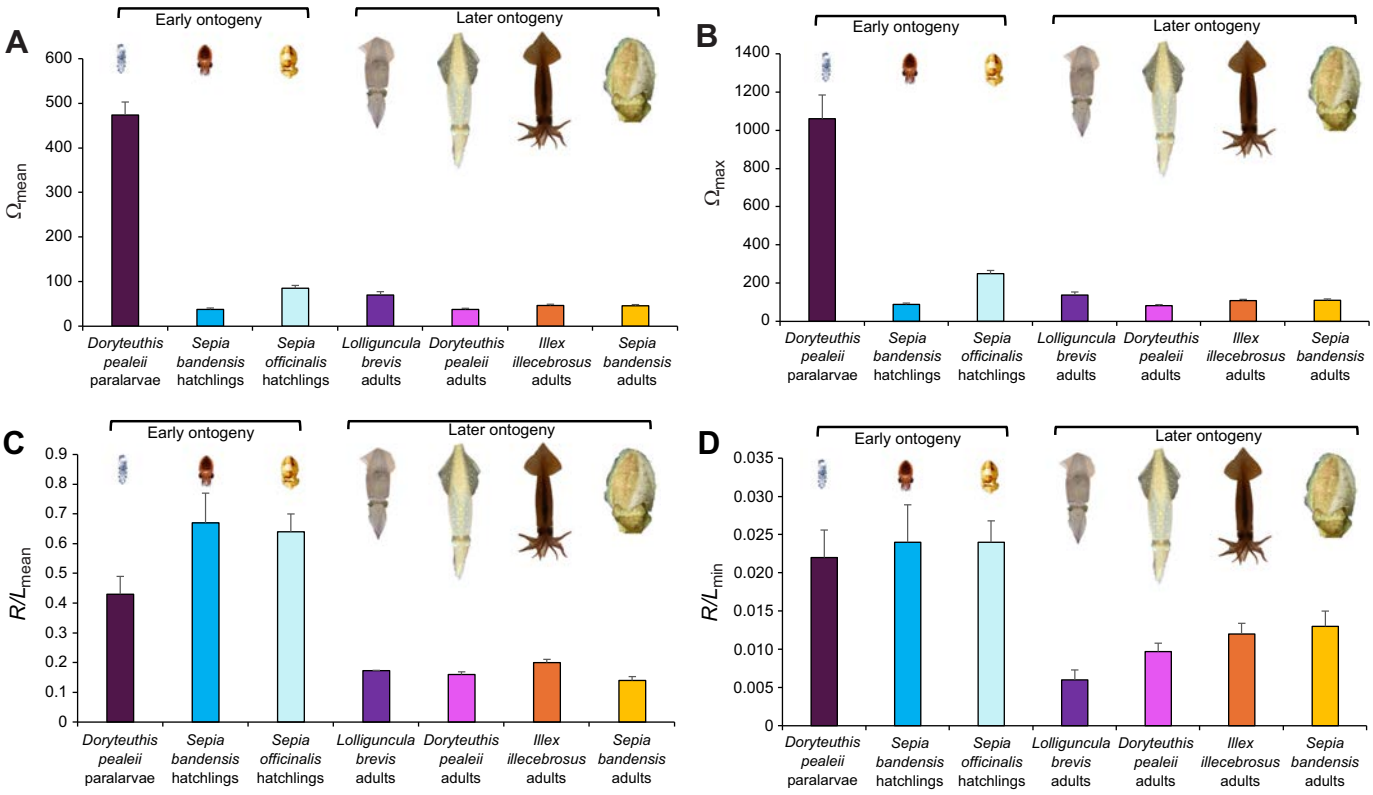

Fig. 8. Kinematic turning variable comparisons among cephalopods. Mean and maximum angular velocity (Ω_{mean}, Ω_{max}; A,B) and mean and minimum length-specific turning radius (R/L_{mean}, R/L_{min}; C,D). Data for *Sepia bandensis* and *Sepia officinalis* hatchlings from Ganley et al. (2024), *Lolliguncula brevis* adults from Bartol et al. (2022), *Doryteuthis pealeii* and *Illex illecebrosus* adults from Ganley et al. (2023), and *S. bandensis* adults from A.M.G., P.S.K. and I.K.B. (unpublished data).

when living in the cuttlefish's more benthic habitat compared with the epipelagic zone, where squid paralarvae reside and where predatory threats are more omnidirectional.

Hatchling dwarf cuttlefish, *S. bandensis*, turn with Ω_{mean}=38 deg s^{-1} and Ω_{max}=89 deg s^{-1}; this is significantly slower than hatchling common cuttlefish, *S. officinalis*, which turn with Ω_{mean}=85 deg s^{-1} and Ω_{max}=250 deg s^{-1} (Ganley et al., 2024). In comparison, squid *D. pealeii* paralarvae turned at much higher angular velocities, with Ω_{mean}=474 deg s^{-1} and Ω_{max}=1060 deg s^{-1} in the present study (Fig. 8A,B). Higher Ω for squid paralarvae is reasonable given their smaller size (~3.5 mm *L*) compared with larger cuttlefish hatchlings (9.2–9.6 mm *L*), as smaller animals have lower moments of inertia and higher Ω than larger swimmers (Fish and Holzman, 2019; Fish et al., 2018). In contrast to *S. officinalis* and *S. bandensis* hatchlings, *D. pealeii* paralarvae exhibited a greater preference for TF turning (95% of turns were TF compared with 56–61% of turns for cuttlefish hatchlings; Ganley et al., 2024), which is consistent with TF swimming preferences reported in other squid paralarvae studies (Bartol et al., 2009b; Vidal et al., 2018; Zakroff et al., 2018). Given the fins play an integral propulsive role during AF swimming in juvenile and adult squids (Bartol et al., 2001, 2016; Stewart et al., 2010), this behavioral preference may derive from the rudimentary fins contributing minimal thrust at this life stage.

Adult cephalopods turn more tightly but more slowly compared with paralarval *D. pealeii* (Fig. 8). Adult brief squid, *L. brevis*, turn with R/L_{mean}=0.17 and R/L_{min}=0.006 during routine turning (Bartol et al., 2022) and even lower *R*/*L* (R/L_{mean}=0.009 and R/L_{min}=0.003) when induced to turn with tethered prey (Jastrebsky et al., 2016). For adult *L. brevis*, Ω_{mean} and Ω_{max} range from 36 to 110 deg s^{-1} and 138 to 303 deg s^{-1}, respectively, with the absolute highest Ω_{max} of 775 deg s^{-1} (Bartol et al., 2022; Jastrebsky et al., 2016, 2017). Other adult squids, such as *D. pealeii* and *I. illecebrosus*, generally exhibit lower agility and maneuverability than adult *L. brevis*, with R/L_{mean}=0.15–0.20, R/L_{min}=0.0097–0.022, Ω_{mean}=27–47 deg s^{-1} and Ω_{max}=71–109 deg s^{-1} (Bartol et al., 2023; Ganley et al., 2023). Adult cuttlefish *S. bandensis* have R/L_{mean}=0.095–0.14, R/L_{min}=0.0012–0.013, Ω_{mean}=46–55 deg s^{-1} and Ω_{max}=110–160 deg s^{-1}, with the absolute highest Ω_{max} of 910 deg s^{-1} (Jastrebsky et al., 2016; A.M.G., P.S.K. and I.K.B., unpublished data). R/L_{mean} and R/L_{min} reported above for adult cephalopods fall below those observed for *D. pealeii* paralarvae in the present study, indicating that young squid have lower maneuverability than cephalopods at later ontogenetic stages. This may be related to cephalopods developing more advanced neuromuscular systems as they age (Gilly et al., 1991; Thompson et al., 2010), or simply that tight turning targets are harder to achieve at smaller sizes. Conversely, the observed Ω_{mean} and Ω_{max} for *D. pealeii* paralarvae exceeded those reported above, and thus *D. pealeii* paralarvae enjoy much higher agility than older cephalopods. Based on the size effects described above, this finding is not surprising. However, it does raise the question of why such high angular velocities (>2000 deg s^{-1}) are needed. Perhaps high Ω are important for evading the myriad predators encountered during the critical post-hatch paralarval phase, where young squid must avoid predators while learning to capture prey, all before yolk reserves are depleted (Robin et al., 2014; Vidal and Shea, 2023; Vidal et al., 2018). Or these extreme angular velocities, including one angular velocity turn >7000 deg s^{-1}, are simply a product of poor control

systems during early ontogeny, where deceleration of spins is difficult to achieve once high turning rates are set in motion.

Jet angular impulse and turning performance

As predicted in hypothesis 2, greater **A** contributed to higher Ω_{mean}, as well as greater angular displacement. This finding is consistent with patterns observed in adult brief squid *L. brevis* (Bartol et al., 2022). In the present study, angular displacement was also dependent on Ω, which is logical, as higher Ω leads to more angular displacement because the animal goes through a larger angle for a given acceleration and deceleration period. Interestingly, lower **A** was not consistently associated with lower *R*/*L*, suggesting that paralarvae that produce high jet **A** can also achieve tight turns. Indeed, while some paralarvae used jets of lower **A** to keep *R*/*L* low (e.g. Fig. 7F), other paralarvae employed vectored jets of high **A** to achieve low *R*/*L* (e.g. Fig. 7G). In addition to jet vectoring, arm angle manipulation (e.g. Fig. 1C,D) may have also facilitated tight turns, even at intermediate to high **A**, reflecting the complexity of the squid system.

Reynolds number, jet wake topology and turning performance

Reynolds number (Re_{squid}) was relevant for kinematic turning parameters, with lower R/L_{mean} occurring at lower Re_{squid} and higher Ω_{mean} occurring at higher Re_{squid}. These results suggest that viscosity may aid squid paralarvae in completing tight turns (greater viscosity will limit drift/coasting), while increases in relative inertial effects can benefit paralarvae when making fast turns (limited viscous effects promote faster swimming) (Vogel, 2013). Some turns involved inducement of water movement near the mantle, head and arms during rotation, which was likely the result of the relatively high viscosity fluid environment at low and intermediate *Re*.

The *Re* threshold reported for effective swimming in other jetting animals occurs at ∼5 based on theoretical estimates (Herschlag and Miller, 2011) and at ∼9 based on experimental data (Katija and Jiang, 2013). Using numerical methods, Herschlag and Miller (2011) reported that forward velocities approach zero for jellyfish when *Re* is <10, with vorticity quickly dissipating at the end of each contraction and expansion of the bell margin when *Re* is <4. For jellyfish *Sarsia tubulosa* and *Aurelia aurita*, the lower threshold of *Re* is ∼13–16 (Herschlag and Miller, 2011; Katija et al., 2015), which is consistent with the reported Re_{squid} lower bound (14) for the present study. Based on experimental studies of *S. tubulosa* with a ∼1 mm velar diameter, mean Re_{jet} is 15, with Re_{jet}=9 being the lowest value detected (Katija and Jiang, 2013). For the present study, some jets with vortex ring formation were observed at Re_{jet}<5 (Fig. 5B), and many jets (24%) occurred at Re_{jet}<6, suggesting that squid paralarvae operate very close to and even below the *Re* thresholds observed in other jet-propelled swimmers. The ability of squid paralarvae to produce vortical structures nearer to the viscous dominated condition of *Re*<1 than other jetters may derive from funnel aperture changes (Dabiri et al., 2006) or vortex stretching (Herschlag and Miller, 2011). Additionally, the valve structure for flow intake and ejection in squid relieves them from constraints of the scallop theorem that tend to drive performance reduction in swimmers with simpler anatomy, such as jellyfish (Herschlag and Miller, 2011), when *Re* is reduced.

Cuttlefish hatchlings and squid paralarvae exhibit similar jet characteristics during turns, with both taxa producing jet mode I (isolated vortex rings) and jet mode II (longer jets often with a leading-edge vortex ring structure). Mean L_ω/D_ω values for cuttlefish hatchlings *S. bandensis* and *S. officinalis* are 2.6–4.1 (Ganley et al., 2024). Of the two cuttlefishes considered, Ganley et al. (2024) found that *S. officinalis* produced faster, yet shorter jets than *S. bandensis*, allowing *S. officinalis* to turn with higher Ω but similar *R*/*L*. The observed mean L_ω/D_ω for paralarval squid in the present study (L_ω/D_ω=3.2) fell within the range reported for cuttlefish hatchlings. Squid paralarvae did operate in a lower *Re* range, however, where Re_{animal} for squid paralarvae was ∼10–700 and Re_{animal} for cuttlefish hatchlings was ∼10–5500.

Not surprisingly, there are some differences in jet flow dynamics for *D. pealeii* paralarvae during station holding (vertical bobbing) versus turning. Although mean L_ω/D_ω was similar for the two activities (L_ω/D_ω=3.2 for turning, L_ω/D_ω=3.6 for station holding), the range of L_ω/D_ω for turns was greater (L_ω/D_ω range for turning=1.8–8.3, L_ω/D_ω range for station holding=2.1–4.6) (Bartol et al., 2009b). Given that a broader range of behaviors was studied in the present study (i.e. tight and broad turns, slow and fast turns, etc., versus station holding), a larger span of L_ω/D_ω is reasonable. Like jet flows observed during station holding, viscous diffusion seemingly blurred and/or pre-empted distinct separation of the leading vortex ring from the trailing jet for paralarvae during many turns. However, for some long jets, evidence of a separated leading-edge vortex ring structure (e.g. Fig. 4D/H) or a pronounced leading-edge ring structure with a much weaker vorticity tail (e.g. Fig. 3D/H) was observed, which was also reported in Bartol et al. (2009b). The observed ranges of U_{jave} (6–72 mm s^{-1}) and U_{jmax} (13–129 mm s^{-1}) for the present study are in reasonable agreement with those reported by Bartol et al. (2009b) for station holding (U_{jave}: 10–50 mm s^{-1}, U_{jmax}: 20–120 mm s^{-1}). In a study examining the effects of ocean acidification on paralarval squid behavior, Zakroff et al. (2018) report U_{jave}=14.7–17.6 mm s^{-1} during vertical swimming, which is also close to the U_{jave} in the present study (22.3 mm s^{-1}).

Although a wide range of jet flows was observed, with both jet modes I and II being prominent, no strong relationship between L_ω/D_ω and either *R*/*L* or Ω was detected, i.e. shorter jets were not strongly associated with tight, controlled turns, and longer jets did not reliably drive broad, fast turns. While a significant linear regression of *R*/*L* on L_ω/D_ω was observed, the R^2 value was low (<7%), suggesting jet length-to-diameter ratios are not good predictors of turning radius. This finding is consistent with the performance of some adult cephalopods, including brief squid, *L. brevis* (Bartol et al., 2022), and shortfin squid, *I. illecebrosus* (Bartol et al., 2023), where consistent relationships between L_ω/D_ω and either *R*/*L* or Ω were not detected. Conversely, adult longfin squid, *D. pealeii*, exhibit elevated *R*/*L* with increased L_ω/D_ω (R^2=0.34) (Bartol et al., 2023). The stronger *D. pealeii* adult relationship between *R*/*L* and L_ω/D_ω may relate to the broader range of L_ω/D_ω recorded in *D. pealeii* adults (∼2–25) versus paralarvae (∼2–8), as some of the high L_ω/D_ω values played an integral role in the regression. The absence of a strong relationship between L_ω/D_ω and either *R*/*L* or Ω in paralarvae suggests that multiple jet pulse approaches (e.g. short or long) may be employed to achieve either high agility or maneuverability. For example, short jets (low L_ω/D_ω) may be directed in precise pulses for controlled turns (low *R*/*L*) (Fig. 7A) or in rapid succession for fast turns (high Ω) (Fig. 7B). Long jets (high L_ω/D_ω) with rapid vectoring may promote high agility (high Ω) (Fig. 7D), whereas long jets with slow but significant sweeping motions can lead to greater control and improved maneuverability (low *R*/*L*) (Fig. 7E). In addition to L_ω/D_ω, jet frequency and level of vectoring, squid paralarvae can adjust jet velocity, angular impulse and body/arm positioning as mentioned above, resulting in a complex multi-layered system for turning.

The absence of a strong relationship between Ω_{mean} and *R*/*L* was unexpected, as controlling *R*/*L* should become increasing difficult

as Ω_{mean} and inertia increase. Linear relationships between these metrics have been observed in the siphonophore *Nanomia bijuga* and adult squids *D. pealeii* and *I. illecebrosus* (Ganley et al., 2023; Sutherland et al., 2019b). The absence of a relationship in paralarval *D. pealeii* indicates that young squid can turn both quickly and tightly when needed, a pattern also observed in the highly maneuverable adult brief squid, *L. brevis* (Bartol et al., 2022).

Caveats and future directions

There are several limitations to the current study. First, the dataset may be biased toward TF turning. While TF turning was clearly the preferred mode, AF turns were likely underrepresented. This is because the funnel undergoes significant curvature and is angled more during AF turns, resulting in jet flows that are less parallel to the laser plane. This, together with greater body interference at the trailing edge (mantle trails during AF turns, shorter arms trail during TF turns), made the jet flow field less resolvable and thus more likely to be excluded from analysis than TF turns. Second, the 2D approach has constraints. Because the funnel can be angled and adjusted during jet ejections, it is likely that the laser plane did not fully bisect the jet in all cases. The 2D approach also does not capture the full behavioral extent of paralarval turns, such as spiral and corkscrew turns that involve multi-plane rotation. Third, flow entrainment from the body (drag) can affect angular impulse calculations. Care was taken to tightly define the jet component of the flow field during processing and to consider frames with the most developed jet flows located away from the body, but some body flows may have contaminated the angular impulse calculations. Fourth, the laser thickness (~1–1.5 mm) was large relative to the paralarva's funnel, which can lead to over-averaging of velocities if adjustments are not performed. For this study, we employed a deconvolution approach, and our data indicate that the conventional DPIV method significantly underestimates jet velocities if deconvolution is not employed. While the deconvolution approach corrects for over averaging, it assumes axisymmetry, which may not be the case for all jets. However, most jet flows were axisymmetric for this study, with observed asymmetry being largely a product of body-induced flows that were mostly excluded from angular impulse calculations. This differs from wakes of other turning jetters, such as jellyfish, where vortices can diverge significantly from axisymmetry (Costello et al., 2021, 2024). In cases where asymmetry is prominent, other approaches besides deconvolution may be advantageous, such as brightfield micro-particle image velocimetry (μPIV) (Gemmell et al., 2014; Karakas et al., 2020).

Research on squid paralarvae and other larval swimmers can be appreciably advanced with new 3D volumetric approaches. In recent years, there has been significant development in 3D flow quantification software and hardware, including advancements in vector resolution within imaging voxels, dynamic object tracking, and camera probes that can accommodate a wider range of lenses (Schanz et al., 2016, 2021; Wieneke and Rockstroh, 2024). These advances promise to complement current 2D approaches by providing a more global picture of flow features. More significantly, a fully 3D flow quantification platform could address many of the limitations described above, as it has the potential to resolve highly angled jet flows, consider turning behaviors that fall outside of 2D planes, and potentially overcome some of the over-averaging effects of conventional DPIV.

Summary

Squid paralarvae turned with higher agility (Ω) but lower maneuverability (R/L) than later ontogenetic stages, and paralarvae exceeded cuttlefish hatchlings in turning performance, in terms of both Ω and R/L. In ~8% of turns, squid paralarvae reached Ω_{max} exceeding 2000 deg s^{-1}, with one squid reaching 7600 deg s^{-1}, which is among the fastest angular velocities recorded for an aquatic animal. Greater **A** produced higher Ω and total angular displacement, and both Ω and R/L increased with higher Re_{squid} as relative inertial effects became larger. Squid paralarvae produced a diversity of jet flows, including isolated vortex rings (jet mode I) and longer vorticity structures with and without leading edge ring elements (jet mode II), and for some turns, movements of the body/arms induced significant flow, which was presumably a consequence of greater viscous entrainment at low/intermediate *Re*. Squid jets were often produced at low *Re* (24% of Re_{jet} fell below 6) with some even approaching the viscous dominated domain of $Re<1$ (lowest recorded $Re_{jet}=3$), but they still demonstrated typical vortical structures upon jet ejection. Unexpectedly, L_ω/D_ω was not strongly predictive of turning performance. This study demonstrates that turning performance of squid paralarvae depends on a combination of multiple elements, and young squid employ a range of jet approaches to turn effectively.

Acknowledgements

We thank Amanda Tumminelli for valuable assistance during data collection and the undergraduate research assistants, Elaine Walters, John Paul Cross, Jason Dunphy, Cathryn Bowling and Darya Bartol, for assistance during data processing.

Competing interests

The authors declare no competing or financial interests.

Author contributions

Conceptualization: I.K.B., P.S.K., J.T.T.; Data curation: I.K.B.; Formal analysis: I.K.B.; Funding acquisition: I.K.B., P.S.K., J.T.T.; Investigation: I.K.B., A.M.G.; Methodology: I.K.B.; Project administration: I.K.B.; Resources: I.K.B.; Software: I.K.B., P.S.K.; Supervision: I.K.B.; Validation: I.K.B.; Visualization: I.K.B.; Writing – original draft: I.K.B.; Writing – review & editing: I.K.B., A.M.G., P.S.K., J.T.T.

Funding

This project was supported by the National Science Foundation (IOS 1557669, 1557698 and 1557838 to I.K.B., P.S.K. and J.T.T.).

Data and resource availability

Datasets and code used in this study are available upon request from the authors.

References

Anderson, E. and Demont, M. E. (2005). The locomotory function of the fins in the squid *Loligo pealei*. *Mar. Freshw. Behav. Physiol.* **38**, 169-189. doi:10.1080/10236240500230765

Bartol, I. K., Patterson, M. R. and Mann, R. (2001). Swimming mechanics and behavior of the shallow-water brief squid *Lolliguncula brevis*. *J. Exp. Biol.* **204**, 3655-3682. doi:10.1242/jeb.204.21.3655

Bartol, I. K., Krueger, P. S., Thompson, J. T. and Stewart, W. J. (2008). Swimming dynamics and propulsive efficiency of squids throughout ontogeny. *Integr. Comp. Biol.* **48**, 720-733. doi:10.1093/icb/icn043

Bartol, I. K., Krueger, P. S., Stewart, W. J. and Thompson, J. T. (2009a). Hydrodynamics of pulsed jetting in juvenile and adult brief squid *Lolliguncula brevis*: evidence of multiple jet 'modes' and their implications for propulsive efficiency. *J. Exp. Biol.* **212**, 1889-1903. doi:10.1242/jeb.027771

Bartol, I. K., Krueger, P. S., Stewart, W. J. and Thompson, J. T. (2009b). Pulsed jet dynamics of squid hatchlings at intermediate Reynolds numbers. *J. Exp. Biol.* **212**, 1506-1518. doi:10.1242/jeb.026948

Bartol, I. K., Krueger, P. S., Jastrebsky, R. A., Williams, S. and Thompson, J. T. (2016). Volumetric flow imaging reveals the importance of vortex ring formation in squid swimming tail-first and arms-first. *J. Exp. Biol.* **219**, 392-403. doi:10.1242/jeb.129254

Bartol, I. K., Ganley, A. M., Tumminelli, A. N., Krueger, P. S. and Thompson, J. T. (2022). Vectored jets power arms-first and tail-first turns differently in brief squid with assistance from fins and keeled arms. *J. Exp. Biol.* **225**, jeb244151. doi:10.1242/jeb.244151

Bartol, I. K., Ganley, A. M., Tumminelli, A. N., Bartol, S. M., Thompson, J. T. and Krueger, P. S. (2023). Turning performance and wake dynamics of neritic squids. *Mar. Biol.* **170**, 73. doi:10.1007/s00227-023-04214-3

Blake, R. W., Chatters, L. M. and Domenici, P. (1995). Turning radius of yellowfin tuna (*Thunnus albacares*) in unsteady swimming manoeuvres. *J. Fish Biol.* **46**, 536-538. doi:10.1111/j.1095-8649.1995.tb05994.x

Cantwell, B. J. (1986). Viscous starting jets. *J. Fluid Mech.* **173**, 159-189. doi:10.1017/S002211208600112X

Costello, J. H., Colin, S. P., Dabiri, J. O., Gemmell, B. J., Lucas, K. N. and Sutherland, K. R. (2021). The hydrodynamics of jellyfish swimming. *Annu. Rev. Mar. Sci.* **13**, 375-396. doi:10.1146/annurev-marine-031120-091442

Costello, J. H., Colin, S. P., Gemmell, B. J., Dabiri, J. O. and Kanso, E. A. (2024). Turning kinematics of the scyphomedusa *Aurelia aurita*. *Bioinspir. Biomim.* **19**, 026005. doi:10.1088/1748-3190/ad1db8

Dabiri, J. O., Colin, S. P. and Costello, J. H. (2006). Fast-swimming hydromedusae exploit velar kinematics to form an optimal vortex wake. *J. Exp. Biol.* **209**, 2025-2033. doi:10.1242/jeb.02242

Dabiri, J. O., Colin, S. P., Gemmell, B. J., Lucas, K. N., Leftwich, M. C. and Costello, J. H. (2020). Jellyfish and fish solve the challenges of turning dynamics similarly to achieve high maneuverability. *Fluids* **5**, 106. doi:10.3390/fluids5030106

Danos, N. and Lauder, G. V. (2007). The ontogeny of fin function during routine turns in zebrafish *Danio rerio*. *J. Exp. Biol.* **210**, 3374-3386. doi:10.1242/jeb.007484

Dickel, L., Chichery, M.-P. and Chichery, R. (1998). Time differences in the emergence of short- and long-term memory during post-embryonic development in the cuttlefish, *Sepia*. *Behav. Process.* **44**, 81-86. doi:10.1016/S0376-6357(98)00024-2

Dickel, L., Chichery, M. and Chichery, R. (2001). Increase of learning abilities and maturation of the vertical lobe complex during postembryonic development in the cuttlefish, *Sepia*. *Dev. Psychobiol. J. Int. Soc. Dev. Psychobiol.* **39**, 92-98. doi:10.1002/dev.1033

Dickel, L., Darmaillacq, A.-S., Jozet-Alves, C. and Bellanger, C. (2013). Learning, memory, and brain plasticity in cuttlefish (*Sepia officinalis*). In *Handbook of Behavioral Neuroscience* (ed. R. Menzel and P. R. Benjamin), pp. 318-333. Elsevier.

Domenici, P. and Blake, R. W. (1997). The kinematics and performance of fish fast-start swimming. *J. Exp. Biol.* **200**, 1165-1178. doi:10.1242/jeb.200.8.1165

Fish, F. E. and Holzman, R. (2019). Swimming turned on its head: stability and maneuverability of the shrimpfish (*Aeoliscus punctulatus*). *Integr. Org. Biol.* **1**, obz025. doi:10.1093/iob/obz025

Fish, F. E., Hurley, J. and Costa, D. P. (2003). Maneuverability by the sea lion *Zalophus californianus*: turning performance of an unstable body design. *J. Exp. Biol.* **206**, 667-674. doi:10.1242/jeb.00144

Fish, F. E., Kolpas, A., Crossett, A., Dudas, M. A., Moored, K. W. and Bart-Smith, H. (2018). Kinematics of swimming of the manta ray: three-dimensional analysis of open-water maneuverability. *J. Exp. Biol.* **221**, jeb166041. doi:10.1242/jeb.166041

Flaspohler, G. E., Caruso, F., Mooney, T. A., Katija, K., Fontes, J., Afonso, P. and Shorter, K. A. (2019). Quantifying the swimming gaits of veined squid (*Loligo forbesii*) using bio-logging tags. *J. Exp. Biol.* **222**, jeb198226. doi:10.1242/jeb.198226

Ganley, A. M., Krueger, P. S. and Bartol, I. K. (2023). Faster is not always better: turning performance trade-offs in the inshore squids *Doryteuthis pealeii* and *Illex illecebrosus*. *J. Exp. Mar. Biol. Ecol.* **565**, 151913. doi:10.1016/j.jembe.2023.151913

Ganley, A. M., Bartol, I. K. and Krueger, P. S. (2024). Baby's first jets: a kinematic and hydrodynamic analysis of turning in cuttlefish hatchlings. *Mar. Biol.* **171**, 221. doi:10.1007/s00227-024-04515-1

Gemmell, B. J., Jiang, H. and Buskey, E. J. (2014). A new approach to micro-scale particle image velocimetry (μPIV) for quantifying flows around free-swimming zooplankton. *J. Plankton Res.* **36**, 1396-1401. doi:10.1093/plankt/fbu067

Gemmell, B. J., Troolin, D. R., Costello, J. H., Colin, S. P. and Satterlie, R. A. (2015). Control of vortex rings for manoeuvrability. *J. R. Soc. Interface* **12**, 20150389. doi:10.1098/rsif.2015.0389

Gemmell, B. J., Dabiri, J. O., Colin, S. P., Costello, J. H., Townsend, J. P. and Sutherland, K. R. (2021). Cool your jets: biological jet propulsion in marine invertebrates. *J. Exp. Biol.* **224**, jeb222083. doi:10.1242/jeb.222083

Gerstner, C. L. (1999). Maneuverability of four species of coral-reef fish that differ in body and pectoral-fin morphology. *Can. J. Zool.* **77**, 1102-1110. doi:10.1139/z99-086

Gharib, M., Rambod, E. and Shariff, K. (1998). A universal time scale for vortex ring formation. *J. Fluid Mech.* **360**, 121-140. doi:10.1017/S0022112097008410

Gilly, W. F., Hopkins, B. and Mackie, G. O. (1991). Development of giant motor axons and neural control of escape responses in squid embryos and hatchlings. *Biol. Bull.* **180**, 209-220. doi:10.2307/1542390

Gladman, N. W. and Askew, G. N. (2023). The hydrodynamics of jet propulsion swimming in hatchling and juvenile European common cuttlefish, *Sepia officinalis*. *J. Exp. Biol.* **226**, jeb246225. doi:10.1242/jeb.246225

Goldbogen, J. A., Calambokidis, J., Friedlaender, A. S., Francis, J., DeRuiter, S. L., Stimpert, A. K., Falcone, E. and Southall, B. L. (2013). Underwater acrobatics by the world's largest predator: 360° rolling manoeuvres by lunge-feeding blue whales. *Biol. Lett.* **9**, 20120986. doi:10.1098/rsbl.2012.0986

Hanlon, R. T. and Messenger, J. B. (2018). *Cephalopod Behaviour*, 2nd edn. Cambridge: Cambridge University Press.

Harada, N. and Tanaka, H. (2022). Kinematic and hydrodynamic analyses of turning manoeuvres in penguins: body banking and wing upstroke generate centripetal force. *J. Exp. Biol.* **225**, jeb244124. doi:10.1242/jeb.244124

Hedrick, T. L. (2008). Software techniques for two-and three-dimensional kinematic measurements of biological and biomimetic systems. *Bioinspir. Biomim.* **3**, 034001. doi:10.1088/1748-3182/3/3/034001

Herschlag, G. and Miller, L. (2011). Reynolds number limits for jet propulsion: a numerical study of simplified jellyfish. *J. Theor. Biol.* **285**, 84-95. doi:10.1016/j.jtbi.2011.05.035

Hoar, J. A., Sim, E., Webber, D. M. and O'Dor, R. K. (1994). The role of fins in the competition between squid and fish. In *The Mechanics and Physiology of Animal Swimming* (ed. J. M. V. Rayner, L. Maddock and Q. Bone), pp. 27-44. Cambridge: Cambridge University Press.

Howland, H. C. (1974). Optimal strategies for predator avoidance: the relative importance of speed and manoeuvrability. *J. Theor. Biol.* **47**, 333-350. doi:10.1016/0022-5193(74)90202-1

Hui, C. A. (1985). Maneuverability of the Humboldt penguin (*Spheniscus humboldti*) during swimming. *Can. J. Zool.* **63**, 2165-2167. doi:10.1139/z85-318

Jastrebsky, R. A., Bartol, I. K. and Krueger, P. S. (2016). Turning performance in squid and cuttlefish: unique dual-mode, muscular hydrostatic systems. *J. Exp. Biol.* **219**, 1317-1326. doi:10.1242/jeb.126839

Jastrebsky, R. A., Bartol, I. K. and Krueger, P. S. (2017). Turning performance of brief squid *Lolliguncula brevis* during attacks on shrimp and fish. *J. Exp. Biol.* **220**, 908-919. doi:10.1242/jeb.144261

Karakas, F., Maas, A. E. and Murphy, D. W. (2020). A novel cylindrical overlap-and-fling mechanism used by sea butterflies. *J. Exp. Biol.* **223**, jeb221499. doi:10.1242/jeb.221499

Katija, K. and Jiang, H. (2013). Swimming by medusae *Sarsia tubulosa* in the viscous vortex ring limit. *Limnol. Oceanogr. Fluids Environ.* **3**, 103-118. doi:10.1215/21573689-2338313

Katija, K., Colin, S. P., Costello, J. H. and Jiang, H. (2015). Ontogenetic propulsive transitions by *Sarsia tubulosa* medusae. *J. Exp. Biol.* **218**, 2333-2343. doi:10.1242/jeb.115832

Leahy, A. M., Fish, F. E., Kerr, S. J., Zeligs, J. A., Skrovan, S., Cardenas, K. L. and Leftwich, M. C. (2021). The role of California sea lion (*Zalophus californianus*) hindflippers as aquatic control surfaces for maneuverability. *J. Exp. Biol.* **224**, jeb243020. doi:10.1242/jeb.243020

Maresh, J. L., Fish, F. E., Nowacek, D. P., Nowacek, S. M. and Wells, R. S. (2004). High performance turning capabilities during foraging by bottlenose dolphins (*Tursiops truncatus*). *Mar. Mammal Sci.* **20**, 498-509. doi:10.1111/j.1748-7692.2004.tb01175.x

Mayerl, C. J., Youngblood, J. P., Rivera, G., Vance, J. T. and Blob, R. W. (2019). Variation in morphology and kinematics underlies variation in swimming stability and turning performance in freshwater turtles. *Integr. Org. Biol.* **1**, oby001. doi:10.1093/iob/oby001

O'Brien, C. E., Mezrai, N., Darmaillacq, A.-S. and Dickel, L. (2017). Behavioral development in embryonic and early juvenile cuttlefish (*Sepia officinalis*). *Dev. Psychobiol.* **59**, 145-160. doi:10.1002/dev.21476

O'Dor, R. K. (1988). The forces acting on swimming squid. *J. Exp. Biol.* **137**, 421-442. doi:10.1242/jeb.137.1.421

Parson, J. M., Fish, F. E. and Nicastro, A. J. (2011). Turning performance of batoids: limitations of a rigid body. *J. Exp. Mar. Biol. Ecol.* **402**, 12-18. doi:10.1016/j.jembe.2011.03.010

Rivera, G., Rivera, A. R. V., Dougherty, E. E. and Blob, R. W. (2006). Aquatic turning performance of painted turtles (*Chrysemys picta*) and functional consequences of a rigid body design. *J. Exp. Biol.* **209**, 4203-4213. doi:10.1242/jeb.02488

Robin, J.-P., Roberts, M., Zeidberg, L., Bloor, I., Rodriguez, A., Briceño, F., Downey, N., Mascaró, M., Navarro, M., Guerra, A. et al. (2014). Chapter Four - Transitions during cephalopod life history: the role of habitat, environment, functional morphology and behaviour. In *Advances in Marine Biology* (ed. E. A. G. Vidal), pp. 361-437. Academic Press.

Saffman, P. G. (1993). *Vortex Dynamics*. Cambridge: Cambridge University Press.

Schanz, D., Gesemann, S. and Schröder, A. (2016). Shake-The-Box: Lagrangian particle tracking at high particle image densities. *Exp. Fluids* **57**, 70. doi:10.1007/s00348-016-2157-1

Schanz, D., Novara, M. and Schröder, A. (2021). Shake-The-Box particle tracking with variable time-steps in flows with high velocity range (VT-STB). In Proceedings of 14th International Symposium on Particle Image Velocimetry (ed. K. T. Christensen), pp. 1-11. Chicago, USA (online): ILLINOIS Tech/Paul V. Galvin Library.

Segre, P. S., Cade, D. E., Calambokidis, J., Fish, F. E., Friedlaender, A. S., Potvin, J. and Goldbogen, J. A. (2019). Body flexibility enhances maneuverability in the world's largest predator. *Integr. Comp. Biol.* **59**, 48-60. doi:10.1093/icb/icy121

Segre, P. S., Gough, W. T., Roualdes, E. A., Cade, D. E., Czapanskiy, M. F., Fahlbusch, J., Kahane-Rapport, S. R., Oestreich, W. K., Bejder, L., Bierlich, K. C. et al. (2022). Scaling of maneuvering performance in baleen whales: larger

whales outperform expectations. *J. Exp. Biol.* **225**, jeb243224. doi:10.1242/jeb.243224

Shea, E. K. and Vecchione, M. (2002). Quantification of ontogenetic discontinuities in three species of oegopsid squids using model II piecewise linear regression. *Mar. Biol.* **140**, 971-979. doi:10.1007/s00227-001-0772-7

Stewart, W. J., Bartol, I. K. and Krueger, P. S. (2010). Hydrodynamic fin function of brief squid, *Lolliguncula brevis*. *J. Exp. Biol.* **213**, 2009-2024. doi:10.1242/jeb.039057

Sutherland, K. R., Gemmell, B. J., Colin, S. P. and Costello, J. H. (2019a). Propulsive design principles in a multi-jet siphonophore. *J. Exp. Biol.* **222**, jeb198242. doi:10.1242/jeb.198242

Sutherland, K. R., Gemmell, B. J., Colin, S. P. and Costello, J. H. (2019b). Maneuvering performance in the colonial siphonophore, *Nanomia bijuga*. *Biomimetics* **4**, 62. doi:10.3390/biomimetics4030062

Sutherland, K. R., Damian-Serrano, A., Du Clos, K. T., Gemmell, B. J., Colin, S. P. and Costello, J. H. (2024). Spinning and corkscrewing of oceanic macroplankton revealed through in situ imaging. *Sci. Adv.* **10**, eadm9511. doi:10.1126/sciadv.adm9511

Sweeney, M. J., Roper, C. F., Mangold, K. M., Clark, M. R. and von Boletzky, S. (1992). "Larval" and juvenile cephalopods: a manual for their identification. *Smithson. Contrib. Zool.* **513**. doi:10.5479/si.00810282.513

Thandiackal, R. and Lauder, G. V. (2020). How zebrafish turn: analysis of pressure force dynamics and mechanical work. *J. Exp. Biol.* **223**, jeb223230.

Thompson, J. T., Bartol, I. K., Baksi, A. E., Li, K. Y. and Krueger, P. S. (2010). The ontogeny of muscle structure and locomotory function in the long-finned squid *Doryteuthis pealeii*. *J. Exp. Biol.* **213**, 1079-1091. doi:10.1242/jeb.034553

Vecchione, M. (1981). Aspects of the early life history of *Loligo pealei* (Cephalopoda: Myopsida). *J. Shellfish Res.* **1**, 171.

Vidal, E. A. G. (1994). Relative growth of paralarvae and juveniles of *Illex argentinus* (Castellanos, 1960) in southern Brazil. *Antarct. Sci.* **6**, 275-282. doi:10.1017/S0954102094000416

Vidal, E. A. G. and Shea, E. K. (2023). Cephalopod ontogeny and life cycle patterns. *Front. Mar. Sci.* **10**, 1162735. doi:10.3389/fmars.2023.1162735

Vidal, E. A. G., Zeidberg, L. D. and Buskey, E. J. (2018). Development of swimming abilities in squid paralarvae: behavioral and ecological implications for dispersal. *Front. Physiol.* **9**, 00954. doi:10.3389/fphys.2018.00954

Vogel, S. (2013). *Comparative Biomechanics: Life's Physical World*, 2nd edn. Princeton University Press.

von Boletzky, S. (1974). The "larvae" of Cephalopoda: a review. *Thalassia Jugoslavica* **10**, 45-76.

Walker, J. A. (1998). Estimating velocities and accelerations of animal locomotion: a simulation experiment comparing numerical differentiation algorithms. *J. Exp. Biol.* **201**, 981-995. doi:10.1242/jeb.201.7.981

Webb, P. W. (1983). Speed, acceleration and manoeuvrability of two teleost fishes. *J. Exp. Biol.* **102**, 115-122. doi:10.1242/jeb.102.1.115

Webb, P. W. and Fairchild, A. G. (2001). Performance and maneuverability of three species of teleostean fishes. *Can. J. Zool.* **79**, 1866-1877. doi:10.1139/z01-146

Weihs, D. and Webb, P. W. (1984). Optimal avoidance and evasion tactics in predator-prey interactions. *J. Theor. Biol.* **106**, 189-206. doi:10.1016/0022-5193(84)90019-5

Wieneke, B. and Rockstroh, T. (2024). Lagrangian particle tracking in the presence of obstructing objects. *Meas. Sci. Technol.* **35**, 055303. doi:10.1088/1361-6501/ad289d

York, C. A. and Bartol, I. K. (2016). Anti-predator behavior of squid throughout ontogeny. *J. Exp. Mar. Biol. Ecol.* **480**, 26-35. doi:10.1016/j.jembe.2016.03.011

Young, R. E. (1988). "Larva", "paralarva", and "subadult" in cephalopod terminology. *Malacologia* **29**, 201-207.

Zakroff, C., Mooney, T. A. and Wirth, C. (2018). Ocean acidification responses in paralarval squid swimming behavior using a novel 3D tracking system. *Hydrobiologia* **808**, 83-106. doi:10.1007/s10750-017-3342-9

Zeidberg, L. and Hamner, W. (2002). Distribution of squid paralarvae, *Loligo opalescens* (Cephalopoda: Myopsida), in the Southern California Bight in the three years following the 1997-1998 El Niño. *Mar. Biol.* **141**, 111-122. doi:10.1007/s00227-002-0813-x